Cavity with a deformable mirror for tailoring the shape of the eigenmode

Peter T. Beyersdorf, Stephan Zappe, M. M. Fejer, and Mark Burkhardt

We demonstrate an optical cavity that supports an eigenmode with a flattop spatial profile—a profile that has been proposed for the cavities in the Advanced Laser Interferometer Gravitational Wave Observatory, the second-generation laser interferometric gravitational wave observatory—because it provides better averaging of the spatially dependent displacement noise on the surface of the mirror than a Gaussian beam. We describe the deformable mirror that we fabricated to tailor the shape of the eigenmode of the cavity and show that this cavity is a factor of 2 more sensitive to misalignments than a comparable cavity with spherical mirrors supporting an eigenmode with a Gaussian profile.

OCIS codes: 220.4000, 350.4600.

1. Introduction

Future interferometric gravitational wave detectors such as the Advanced Laser Interferometer Gravitational Wave Observatory (LIGO)[1] will have a sensitivity in the frequency band of around 100 Hz that is limited by thermal noise of the interferometer mirrors. There are two predominant components to this noise, one that is due to the average temperature of the substrate and coatings that excites all mechanical modes of the mirrors and another called thermoelastic noise[2] that is due to the variance in temperature across the mirror surface that couples through the thermal expansion coefficient of the substrate to produce localized, time-dependent bumps and valleys on the mirror surface. For both sources of noise, if the beam size is larger than the scale of the noise distribution, the noise will be partially averaged out. For thermoelastic noise, the scale of the noise distribution depends on the thermal conductivity of the optical substrate. For sapphire optics, which is an alternative to fused-silica optics for Advanced LIGO, this characteristic size is sufficiently large that the Gaussian beams of the Advanced LIGO baseline design cannot provide enough spatial averaging to reduce the effect of thermoelastic noise below the level of other noise sources at the most sensitive region of the interferometer's response, near 100 Hz. Thus any methods that could improve the spatial averaging of the mirror displacement noise could directly improve the detection sensitivity of future gravitational wave interferometers that use sapphire optics.

To improve the spatial averaging of displacement noise it is advantageous to have the largest spot size on the mirror while meeting the constraint on the allowable diffraction losses due to the edge of the mirror clipping the beam. For the baseline design of Advanced LIGO with 14.9 cm radius mirrors and allowable diffraction losses of 10 parts per million, the largest acceptable Gaussian beam has a radius of 4.23 cm. To further suppress the effect of termoelastic noise, D'Ambrosio *et al.* have proposed the use of non-Gaussian flattop beams[3] in Advanced LIGO to increase the spot size on the mirror. They have calculated a mirror surface profile that will support optical modes with the desired beam shape in the 4 km long arm cavities.[4]

Following the same procedure, we have calculated the mirror profile for a small-scale cavity necessary to generate the equivalent flattop beam. We have fabricated a deformable mirror that can approximate the desired shape and have built a 1.5 m long cavity using this mirror. The mirror's shape is electrostatically controlled and can be dynamically changed, which allowed us to explore the sensitivity of the cavity

P. T. Beyersdorf (pbeyersdorf@science.sjsu.edu) is with the Department of Physics, San José State University, San José, California 95192-0106. S. Zappe, M. M. Fejer, and M. Burkhardt are with the Ginzton Laboratory, Stanford University, Stanford, California 94305-4085.

Received 3 November 2005; revised 1 May 2006; accepted 1 May 2006; posted 4 May 2006 (Doc. ID 65750).

0003-6935/06/266723-06$15.00/0

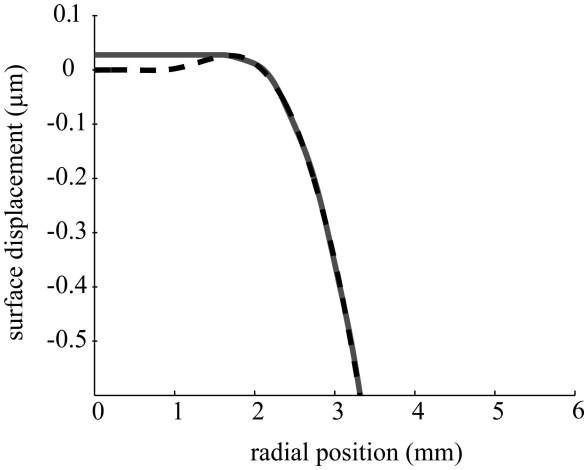

Fig. 1. Ideal mirror shape as calculated (dashed curve) and the shape that can be approximated by an electrostatically actuated flat membrane (solid curve).

Fig. 2. (Color online) Deformable mirror. The circular region in the center of the square is the active region. This central region is a thin membrane that can be distorted by electrostatic actuation from the electrodes underneath. This particular membrane is broken; the bottom half has shattered into many pieces but the top half remains intact.

mode to various misalignments and imperfections to the mirror surface.

2. Calculation of Mirror Shape

The surface profile for the end mirror of our cavity is driven by a number of constraints. Primarily, our cavity must not exceed a few meters in length, so as to fit on an optical table; it must be short compared to the Rayleigh length of the beam so that the mode shape calculated at the waist in the cavity does not differ significantly from the mode shape at the end mirror; and the surface profile for the mirror must have a peak-to-valley difference of less than 6 μm to be achievable with our deformable mirror technology. These constraints lead us to the design of a folded cavity, 1.5 m in length with a 1.8 mm radius waist collocated with a flat mirror that forms one end of the cavity.

To calculate the necessary shape of the deformable mirror, we begin with the desired beam profile at its waist. Following the method of D'Ambrosio *et al.*, we take the amplitude profile of the beam to be the convolution of a rectangle function and a Gaussian beam to give a flattop profile with smoothed edges:

$$U(r > 0) = \exp\left[-\left(\frac{r}{w_c}\right)^2\right] \otimes [1 - H(r - 4w_c)], \quad (1)$$

where $H(r)$ is the Heaviside step function and $w_c = \sqrt{\lambda L/(2\pi)}$ where λ is the wavelength of the light and L is the cavity length.

This mode shape is a flattop with smoothed edges. The smoothed edges allow this profile to propagate with less ripple on the flattop than would be present with hard edges. The calculated amplitude profile is at the beam waist, where the phase profile is flat. This profile represents the beam at one end mirror of the cavity, which is flat to match the phase front of the mode. This mode is decomposed into azimuthally symmetric Laguerre–Gaussian modes. The sum of these modes when evaluated at the other end mirror gives the wavefront at that mirror and also describes the shape of the deformable mirror necessary for this to be a stable mode of the cavity. This ideal mirror shape is shown in Fig. 1.

3. Deformable Mirror

We use a micromachined, electrostatically actuated deformable mirror to achieve the desired mirror surface profile. The basic structure of the device is a flexible silicon nitride membrane coated with a layer of gold to increase the reflectivity. Figure 2 shows the mirror. The membrane sits above a silicon substrate that has electrodes patterned onto the surface for applying localized electrostatic forces to the membrane. Figure 3 shows the electrode pattern and wire layout on the silicon substrate. The gap between the electrodes and the membrane is 20 μm, which gives a

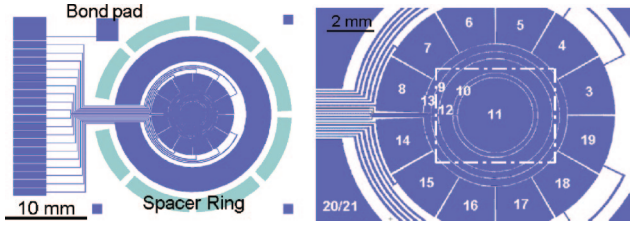

Fig. 3. (Color online) Left, electrode pattern and wire layout on the silicon substrate. Right, closeup of the electrode pattern. Electrodes 9–13 are used to create the desired mirror surface with rotational symmetry. Electrodes 3–8 and 14–19 are used to compensate for saddlelike membrane surface shapes that are typical for as-fabricated mirrors. Electrodes 1 and 2 provide a connection with the membrane through the bond pad. Electrodes 20 and 21 are used to keep the remaining surface area at a defined voltage (usually ground). The nominal silicon nitride membrane diameter is 10 mm and covers all the segmented electrodes and the inner concentric ring and circular electrodes. The area defined by the dotted rectangle was measured by a white-light interferometer to determine the surface profile while the mirror was being deformed.

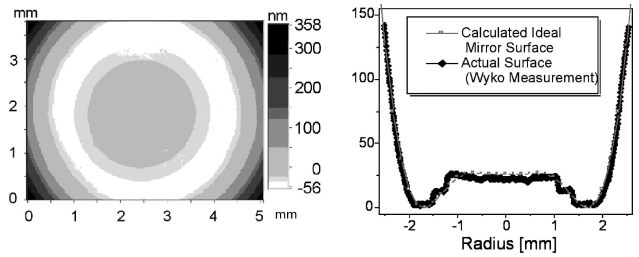

Fig. 4. Left, surface profile of the center of the actuated mirror. Right, the surface height along a cord through the center (solid diamonds) shows that the mirror surface is within 8 nm of the intended surface profile (solid circles) in the central region of the mirror.

dynamic range of 6 μm, beyond which the membrane will snap down onto the substrate.

The electrode pattern on the substrate consists of an outer area containing 12 segmented electrodes and an inner area containing 5 ring electrodes. The outer 12 electrodes are used to correct any residual warping of the unactuated membrane, leaving a flat surface across the central area of the membrane. The ring electrodes then shape the central region into a radially symmetric profile approximating the calculated surface. The radius and width of the five ring actuators were tailored to produce the desired mirror profile using a finite-element model of the displacement of the membrane surface produced by the actuators.

This mirror architecture is inherently limited to producing concave distortions of the membrane because it can only pull on the surface. The desired mirror profile, however, has a convex bump in the center of the mirror. To reproduce the convex portion of the mirror surface with our deformable mirror, a static bump was added to the membrane. This bump consists of two concentric terraces, each 13 nm high, of silicon nitride deposited onto the membrane before it was gold coated. A Wyko NT1100 white-light interferometric optical profiler (Veeco Instruments) was used to measure the membrane shapes of the actuated mirrors. The maximum field of view of our system is approximately 3.8 mm × 5.1 mm. Figure 4 (left side) shows a surface profile of the actuated mirror. The surface height along a cord through the center is plotted on the right and compared with the intended surface height. The static preshaping, along with the dynamically controlled electrostatic actuation, allows the mirror surface to approximate the ideal surface to within 8 nm over the central 6 mm diameter region.

4. Numerical Model of the Cavity

A numerical model of the cavity is used to determine the resonant mode shapes for the cavity. This model allows the effect of deviations from the ideal mirror surface profile to be calculated. The model considers the round-trip propagation of a vector with elements describing the relative amplitude and phase of the Laguerre–Gaussian modes that describe the light circulating in the cavity. The coupling between the modes due to reflection from a mirror of arbitrary surface profile is described by a matrix that has elements given by

$$C_{pmp'm'} = \int_{-\infty}^{\infty} u_{pm}(r,\ \theta,\ L)u_{p'm'}{}^{*}(r,\ \theta,\ L) \times \exp\{-i2k[S(r,\ \theta) - S_0(r,\ \theta)]\} r\,dr\,d\theta. \quad (2)$$

Here p and m are the radial and azimuthal mode numbers, respectively, and the expression represents the coupling from the unprimed mode numbers to the primed mode numbers. $k = 2\pi/\lambda$ is the usual wavenumber, $S(r, \theta)$ is the surface of the deformable mirror, and $S_0(r, \theta)$ is the spherical surface corresponding to the wavefront of the Laguerre–Gaussian beams in this basis. u_{pm} is a Laguerre–Gaussian mode satisfying

$$u_{pm}(r,\ \theta,\ z) = \sqrt{\frac{2p!}{(1+\delta_{0m})\pi(m+p)!}} \times \frac{\exp\{i(2p+m+1)[\psi(z)-\psi_0]\}}{w(z)} \times \left[\frac{\sqrt{2}r}{w(z)}\right]^m L_p{}^m\left[\frac{2r^2}{w^2(z)}\right] \times \exp\left[-ik\,\frac{r^2}{2\tilde{q}(z)} + im\theta\right], \quad (3)$$

where the $L_p{}^m$ functions are the generalized Laguerre polynomials, $w(z)$ is the usual Gaussian beam width, $\psi(z)$ is the Gouy phase, and $\tilde{q}(z)$ is the Gaussian q parameter related to the beam width w and radius of curvature R of the beam by

$$\frac{1}{\tilde{q}(z)} = \frac{1}{R(z)} - i\,\frac{\lambda}{\pi w^2(z)}. \quad (4)$$

For our simulation of the cavity, the input beam is described by a 160 element vector representing the mode amplitude of the first 160 Laguerre–Gaussian modes (10 radial × 16 azimuthal modes), a number of modes that was found to be high enough that the desired mode shape could be well approximated but small enough to avoid stressing the memory or processing capability of the desktop computer running the simulation. One round trip in the cavity is represented by the matrix product of C_1 and C_2, the coupling matrices for each of the cavity end mirrors. The eigenvectors of this round-trip matrix describe the modes of the cavity. We calculate the eigenvectors and add up the profiles of the Laguerre–Gaussian modes with the appropriate amplitude and phase factors from each eigenvector to determine the mode shape of each of the modes. We identify the flattop mode as the mode shape that best fits the intended profile. Figure 5 shows the Gaussian mode shape for a spherically curved mirror and the flattop mode

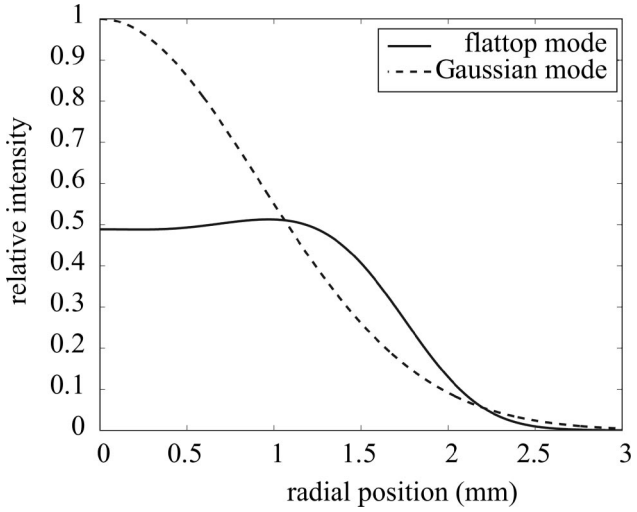

Fig. 5. Calculated eigenmode shapes for a cavity with a spherical mirror (dashed curve) and our deformable mirror (solid curve).

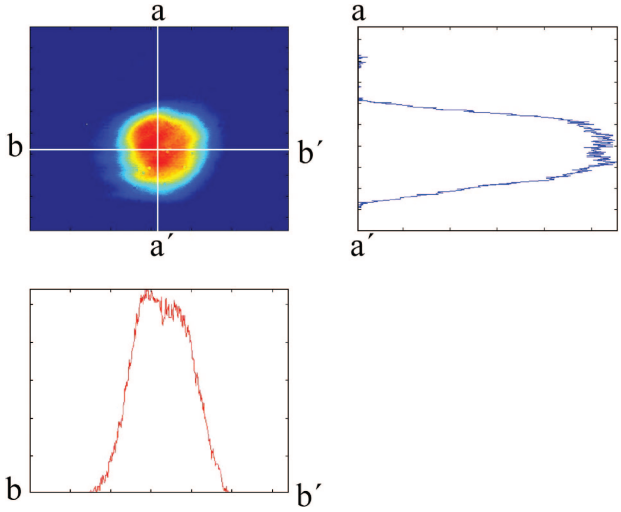

Fig. 7. (Color online) Top left, flattop mode that resonates in the test cavity. The profiles of a chord taken through the middle of the flattop and Gaussian beams are shown in the top right and bottom left plots.

shape for the appropriately deformed mirror that has the surface profile shown in Fig. 5.

5. Optical Cavity with Deformable Mirror

The cavity length is 1.5 m and supports a flattop mode with a full width at half-maximum (FWHM) intensity of 3.8 mm. The input Gaussian beam has a waist at the input coupler to the cavity with a Gaussian beam diameter of 3.6 mm. A flat 99.8% reflectivity mirror is used as the input coupler. The cavity is folded with a high reflector so that its leakage light can be used to monitor the mode shape at the plane of either end mirror. The cavity finesse is 100.

Figure 6 shows the experimental setup of the folded cavity. The deformable mirror surface is monitored by a white-light interferometer while the actuator voltages are adjusted to achieve the desired profile. Once the mirror shape is set, the laser is locked onto the cavity using Pound–Drever–Hall locking. Figure 7 shows the recorded flattop mode shape. By monitoring the transmitted power through the cavity as the length is scanned, we estimate 55% of the power is in the flattop mode.

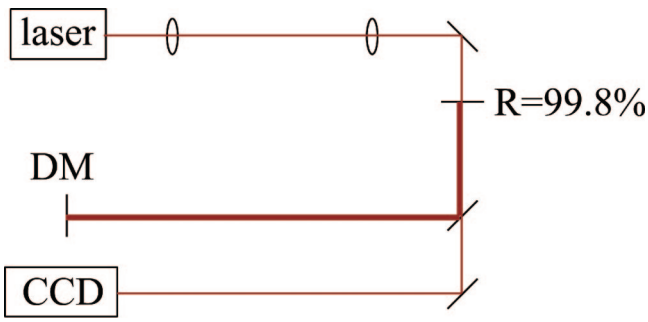

Fig. 6. (Color online) Experimental setup of the optical cavity. A white-light interferometer (not shown) is used to monitor the shape of the deformable mirror (DM).

6. Sensitivity of the Cavity to Perturbations

We introduced several perturbations to the deformable mirror and observed how the stored cavity power and mode shape were affected. A piezoelectric transducer on the mirror mount for the deformable mirror allows fine control of the pitch while the mirror is monitored interferometrically. We performed two experiments with this setup. We monitored the power buildup in the cavity as a function of misalignment angle, and we looked at the change in mode shape as a function of misalignment. We compare our observations with the calculated results for a conventional cavity of equal length but with a spherical mirror instead of the deformable mirror so that it supports a Gaussian mode that has the same FWHM at its waist.

The power in the cavity is plotted as a function of misalignment in Fig. 8 and is compared with that of the conventional cavity. We see that the cavity that supports the flattop mode is twice as sensitive to misalignment as a conventional cavity that supports an equivalent Gaussian mode. It should be noted, however, that in this near-field configuration where the cavity length is short compared to the Rayleigh range of the beam, the conventional cavity itself is only marginally stable with a cavity g parameter of 0.98.

The resonant mode shape also changes with misalignment. We investigated how the change in mode shape would affect the performance of the mode when averaging over the spatially dependent noise on the surface of a mirror. We measured the mode shape as a function of misalignment and used the measured mode shapes, scaled to the size necessary for Advanced LIGO, to weight a simulated noise spectrum that reproduced the behavior of thermoelastic noise in sapphire.

Working with the 720 $\times$ 540 pixel images of the mode shape, we simulate thermoelastic noise by tak-

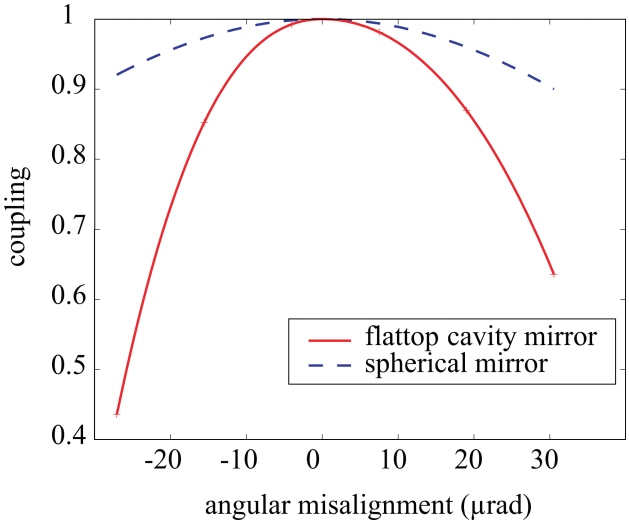

Fig. 8. (Color online) Relative power buildup in the cavity as a function of pitch misalignment of the end mirror. The solid curve fits the measured data for the flattop cavity. The dashed curve is calculated for a conventional cavity. We suspect that the asymmetry of the curve for the flattop cavity is due to transverse displacement of the flattop beam from tilting the cavity end mirror coupling to the misalignment of the monitor photodiode.

ing a 120 × 90 element matrix of random numbers and interpolate it into a 720 × 540 matrix using a cubic spline. This represents displacement noise on the surface of a mirror with a spatial scale that is 4.5% of the FWHM of the illuminating beam (6 pixels relative to our 132 pixel wide beam). The elements of this matrix are used to weight the corresponding pixels of the image of the flattop beam. The elements of the resulting matrix are summed to represent the net displacement noise that would couple to a beam reflecting from a noisy mirror described by this noise matrix. The values for ten different noise matrices are calculated and the root-mean-square value for all ten calculations is used as the estimate for the effect

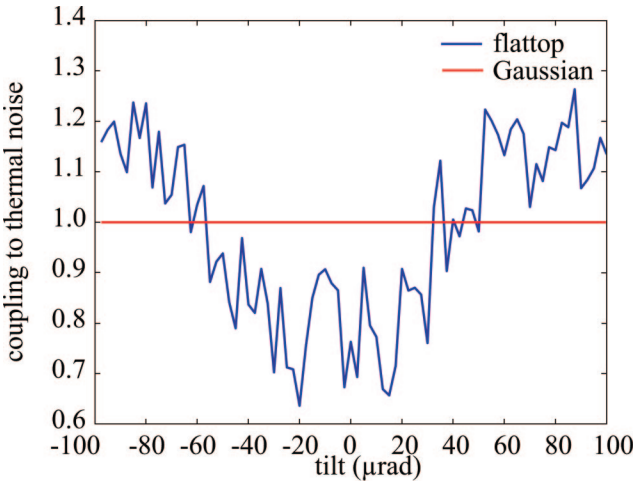

Fig. 9. (Color online) Estimated relative amount of thermoelastic noise that couples to the beam for a flattop beam and a Gaussian beam when the end mirror of the cavity is misaligned.

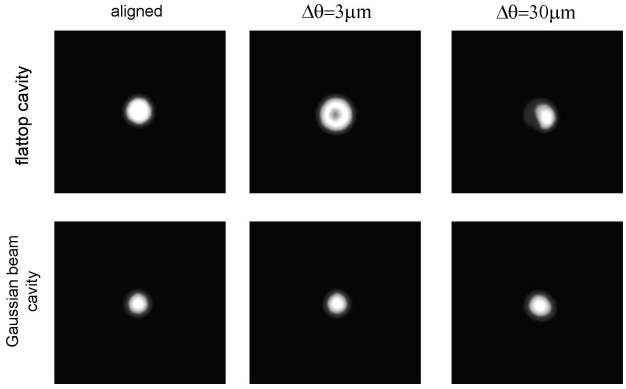

Fig. 10. Calculated cavity mode shapes for a cavity with a deformable mirror (top row) and a spherical mirror (bottom row) for several values of end mirror tilt. The observed mode shapes obey similar behavior; however, the simulated mode-shape images are much cleaner allowing the effect of misalignment to be more easily seen.

of thermoelastic noise in a full-scale interferometer on a beam with the observed shape.

The estimated noise level for the flattop beam was compared with that of a Gaussian beam, which was computed the same way as for the flattop beam, but using an ideal Gaussian profile for the beam rather than the observed beam profile, normalized to have the same width and total power as the observed beam. Figure 9 shows how the expected noise suppression due to the flattop mode shape degrades with misalignment of the cavity end mirror. Figure 10 shows the calculated cavity mode shape for several corresponding values of misalignment of the end mirror.

The signal in a gravitational wave interferometer is directly proportional to the carrier power stored in the arms. From our measurement of the power coupling to the misaligned flattop cavity, we can see that the rate that the signal decreases as the cavity is misaligned is greater than the rate at which thermoelastic noise would increase as the cavity is misaligned, suggesting that the alignment tolerances for the mirrors of a flattop cavity are constrained by the power coupling to the cavity, not by the deformation of the mode shape.

7. Summary

We have used a deformable mirror to modify the mode shape of an optical cavity. The mirror shape necessary for a flattop profile beam was calculated, and a deformable mirror that could achieve this shape was fabricated. The deformable mirror surface was perturbed to explore the effect on the flattop mode that was resonate in the cavity. By monitoring the power transmitted through the cavity and the shape of the resonant mode in the cavity when the end mirror was misaligned, we found that the effect of misalignment is predominantly a change in the power coupling to the cavity, and that this change is twice as great as for a conventional cavity with spherical mirrors supporting the same width eigenmode.

This work was supported by the National Science Foundation grant PHY-0140297, the Stanford Advanced Gravitational Wave Detector Research Program.

References

1. P. Fritschel, "The second generation LIGO interferometers," AIP Conf. Proc. **575,** 15–23 (2001).
2. Y. T. Liu and K. S. Thorne, "Thermoelastic noise and homogeneous thermal noise in finite sized gravitational-wave test masses," Phys. Rev. D **62,** 122002 (2000).
3. E. D'Ambrosio, R. O'Shaughnessy, K. Thorne, P. Willems, S. Strigin, and S. Vyatchanin, "Advanced LIGO: non-Gaussian beams," Class. Quantum Grav. **21,** S867–S873 (2004).
4. E. D'Ambrosio, R. O'Shaughnessy, S. Strigin, K. S. Thorne, and S. Vyatchanin, "Reducing thermoelastic noise in gravitational-wave interferometers by flattening the light beams," *arXiv.org e-Print archive*, gr-qc/0409075, 20 September 2004, http://arxiv.org/abs/gr-qc/0409075.